Improved eigenvalue sums for inferring quantum billiard geometry

1987 J. Phys. A: Math. Gen. 20 2389

(http://iopscience.iop.org/0305-4470/20/9/026)

J. Phys. A: Math. Gen. **20** (1987) 2389-2403. Printed in the UK

Improved eigenvalue sums for inferring quantum billiard geometry

M V Berry

H H Wills Physics Laboratory, University of Bristol, Tyndall Avenue, Bristol BS8 1TL, UK

Received 28 October 1986

Abstract. An algorithm is described for obtaining successive approximations to geometric properties K_j of a closed boundary B (such as its length L or the area A within it), given the lowest N eigenvalues $\{E_n\}$ of some wave operator defined on the domain bounded by B. The technique is based on the asymptotic expansion of the partition function for small t: $\Phi(t) = \sum_{n=1}^{\infty} \exp\{-E_n t\} \sim t^{-1} \sum_{j=0}^{\infty} K_j t^{j/2}$. Four different billiards are employed to illustrate the method. The first is the rectangular membrane, which is classically integrable; for the other three, B is an Africa shape, which is classically chaotic: the Africa membrane, Africa Aharonov-Bohm billiard and Africa neutrino (massless Dirac) billiard. A typical result is that A and L can be reconstructed from 125 eigenvalues to a few parts in 10^4 (for the rectangle the accuracy is even higher). The efficiency of the reconstruction algorithm appears to be independent of the classical chaology of B.

1. Introduction

In quantum billiards, particles satisfying some wave equation move freely inside a finite planar domain whose boundary B has hard walls. Eigenvalues $\{E_n\} = E_1, E_2, \ldots$, are determined by the wave equation together with its boundary conditions (in the simplest case, where the operator $-\nabla^2$ acts on scalar wavefunctions vanishing on B, the $\{E_n\}$ are proportional to the squares of resonant frequencies of elastic membranes clamped round B). Here I explore one aspect of the natural question: can the geometry of B be inferred from knowledge of all or some of the $\{E_n\}$? Or, as Kac (1966) put it, can one hear the shape of a drum?

From $\{E_n\}$ can be constructed the spectral staircase (eigenvalue counting function)

$$N(E) = \sum_{n=1}^{\infty} \theta(E - E_n) \tag{1}$$

where θ denotes the unit step. Because of the steps, $N(E)$ cannot have a convergent power series expansion in E. But the *smoothed* staircase $\langle N(E) \rangle$ does possess an asymptotic expansion for large E:

$$\langle N(E) \rangle = AE/4\pi - \gamma L E^{1/2}/4\pi + C + \ldots . \tag{2}$$

In this equation, A is the area enclosed by B, L is the length of B, and γ and C are constants whose values for three different types of billiard will now be given.

First are the familiar scalar membrane billiards with operator $-\nabla^2$ and Dirichlet boundary conditions, for which (Baltes and Hilf 1976)

$$\gamma = 1 \qquad C = C^{(1)} = \sum_j \int_{B_j} \kappa(s)\, \mathrm{d}s/12 + \sum_i (\pi/\beta_i - \beta_i/\pi)/24 \tag{3}$$

0305-4470/87/092389+15$02.50

where the first summation is over smooth arcs B_j with $\kappa(s)$ being the curvature as function of arc length, and the second summation is over corners with angles β_i. (The assumption here is that B is simply connected and without cusps.) If B is smooth, (3) gives $C^{(1)}=\frac{1}{6}$.

Second are the Aharonov-Bohm billiards (Berry and Robnik 1986) in which quantum time-reversal symmetry is broken by a single line of magnetic flux piercing the domain. If the (dimensionless) flux is α, the operator is $-(\nabla-\mathrm{i}\alpha\boldsymbol{A}(\boldsymbol{r}))^2$ where $\boldsymbol{A}(\boldsymbol{r})$ is any vector potential whose curl is $2\pi\delta(\boldsymbol{r})$ (directed perpendicular to the domain). This operator acts on scalar wavefunctions vanishing on B. Berry (1986) showed that

$$\gamma=1 \qquad C=C^{(2)}=C^{(1)}-\alpha(\mathrm{mod}\ 1)[1-\alpha(\mathrm{mod}\ 1)]/2. \tag{4}$$

Third are the neutrino billiards, where the free massless Dirac operator acts on two-component spinors within B and where the hard wall corresponds to an infinitely high 4-scalar potential. Full details will be given by Berry and Mondragon (1987). For the coefficients in (2) we so far have

$$\gamma=0 \qquad C=C^{(3)} \text{ unknown.} \tag{5}$$

We will be interested in inferring the values of A, L and C (and so distinguishing the three types of billiard) given a sequence of the first N eigenvalues. For this purpose the spectral staircase $N(E)$, employed in conjunction with (2), is not a promising candidate. It is true that, as figure 1 shows, the asymptotic formula is a very accurate description of the smoothed staircase even for small N (and following Berry (1981) is now used routinely to check computations of $\{E_n\}$ for missing eigenvalues). But the fluctuations of the true $N(E)$ about the smoothed $\langle N(E)\rangle$ are large and this makes accurate reconstruction difficult. This is illustrated in figure 2, which shows the deviation of $N(E)$ (taken as $n-\frac{1}{2}$) from equation (2) with C ignored, i.e.

$$\Delta_n=n-\tfrac{1}{2}-AE_n/4\pi-LE_n^{1/2}/4\pi. \tag{6}$$

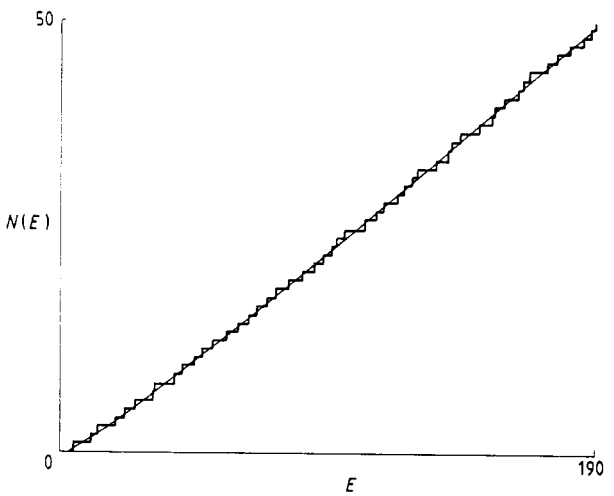

Figure 1. Spectral staircase (1) for first 50 levels of the Africa membrane billiard shown in figure 8; the smooth curve is the asymptotic approximation (2).

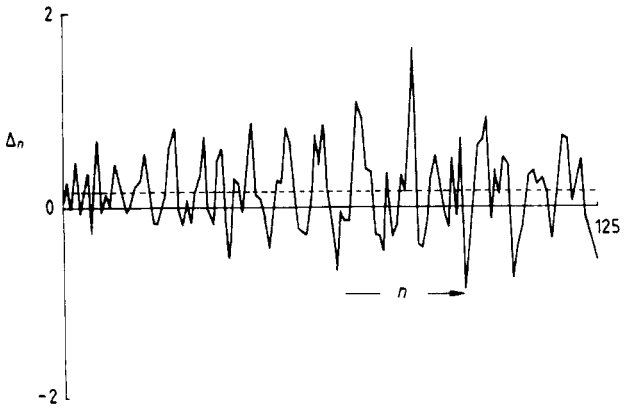

Figure 2. Spectral fluctuations $N(E)-\langle N(E)\rangle$ of the first 125 levels of the staircase of figure 1, calculated using equation (6); the broken line is $C=\frac{1}{6}$.

If A and L are known, the average of Δ_n should give C, in this case $\frac{1}{6}$. However, the fluctuations are several times larger than C so the average gives an inaccurate value: for the data of figure 2, the average is 0.156 and the cumulative averages of the fluctuations, namely $\Sigma_{m=1}^{n}\Delta_m/n$, themselves fluctuate about $C=\frac{1}{6}$ with an amplitude of about $C/5$.

The fluctuations arise from closed orbits (bouncing-ball geodesics) in the billiard domain (Balian and Bloch 1972), which give non-analytic corrections connecting $N(E)$ with $\langle N(E)\rangle$; these are not included in the power series (2). An isolated closed orbit (such as occurs amongst chaotic geodesics), with length l, contributes to $N(E)$ a term of order $\cos(lE^{1/2})$; a non-isolated orbit (such as occurs amongst integrable geodesics) contributes a term greater by a factor $E^{1/4}$. This raises the possibility (Chazarain 1974) of using the fluctuations to infer the length spectrum of the closed geodesics of B. The distribution of closed orbits can also give information about the statistics of the spectral fluctuations (Berry 1985). But when seeking to inder A, L and C from $\{E_n\}$ the fluctuations are a nuisance, and it is best to employ a formalism that avoids them.

One such formalism, to be employed throughout the rest of this paper, is based on the partition function

$$\Phi(t)\equiv\sum_{n=1}^{\infty}\exp\{-E_n t\}. \tag{7}$$

This is t^{-1} times the Laplace transform of the staircase $N(E)$. Corresponding to (2) is an asymptotic expansion for small t which we write formally as

$$\Phi(t)\approx t^{-1}\sum_{j=0}^{\infty}K_j t^{j/2}. \tag{8}$$

The coefficients K_j are related to those in (3):

$$K_0=A/4\pi \qquad K_1=-\gamma L/8\pi^{1/2} \qquad K_2=C. \tag{9}$$

Beyond the term $K_2=C$ (which is 'constant' both for $\Phi(t)$ and $N(E)$) we have in general only the results of Stewartson and Waechter (1971) for smooth scalar flux-free

B, which give, for the first such term

$$K_3 = \int_0^L \mathrm{d}x\, \kappa^2(s)/256\pi^{1/2}. \tag{10}$$

What makes $\Phi(t)$ superior to $N(E)$ as a means of reconstructing billiard geometry is that the fluctuations are exponentially small in t, rather than oscillatory in E: an isolated closed orbit of length l contributes to $\Phi(t)$ a term of order $t^{-1/2}\exp\{-l^2/4t\}$; a non-isolated orbit contributes a similar exponential with t^{-1} replacing $t^{-1/2}$. Figure 3 illustrates how smoothly $\Phi(t)$ is approximated for small t by the first three terms of the asymptotic series (8). Just how good the approximations are in absolute terms is illustrated in figure 4: as they should, the full and broken curves appear to approach $t=0$ as $t^{1/2}$ and t, respectively. Of course, the approximations fail very close to $t=0$ (in fact when $t \lesssim E_{125}^{-1}$) but this is because only 125 eigenvalues (rather than infinitely many) are included in the summation (6), so that $\Phi(0)=125$ (rather than infinity).

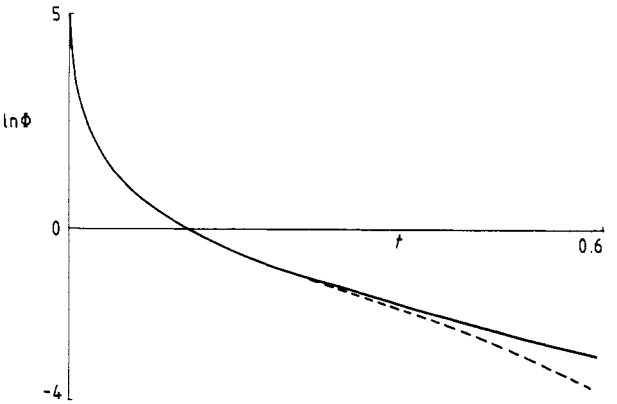

Figure 3. Partition function (7) for the first 125 levels of the Africa membrane billiard shown in figure 8; the broken curve shows the first three terms of the asymptotic approximation (8).

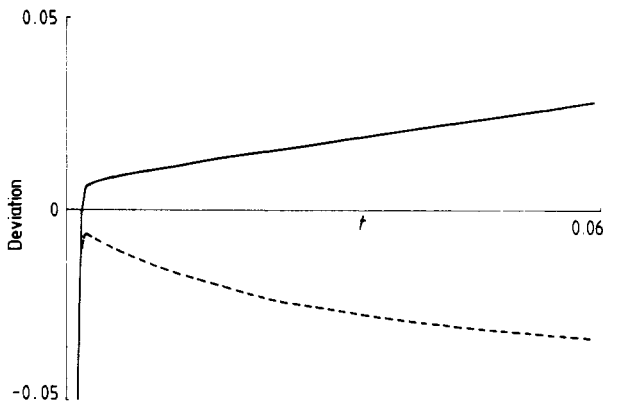

Figure 4. Deviation from $\Phi(t)$ in figure 3 of the first three terms (full curve) and four terms (broken curve) of the approximation (8).

The central idea of this paper (§ 2) is a simple technique for obtaining from the eigenvalues a sequence of improving approximations to each of the constants K_j in (7). The technique is illustrated in § 3 by applying it to reconstructions of A, L and C for four billiards. The first of these is the rectangular membrane. The other three all have B in the Africa shape illustrated in figure 8; for this B we shall study the membrane, Aharonov-Bohm and neutrino billiards.

2. Sums based on the partition function

The obvious way of reconstructing the billiard area from (7)-(9) is through the identity

$$A = 4\pi \lim_{t\to 0} t \sum_{n=1}^{\infty} \exp\{-E_n t\}. \tag{11}$$

But with the finite number of levels available in practice the limit will be zero rather than A (cf corresponding behaviour of $\Phi(t)$ in figure 4), so that the best hope is to approximate A as some kind of plateau in (11) when t is small but not zero. In these circumstances it is important to know how the limit in (11) is approached. From (8) there follows

$$A - 4\pi t \sum_{n=1}^{\infty} \exp\{-E_n t\} \sim t^{1/2} \qquad \text{as } t \to 0. \tag{12}$$

This represents slow convergence to the limit and so we expect (and will later find) bad approximations to A with finitely many levels.

However, convergence to the limit can be systematically improved by defining $t = x^2$ and writing (8) as

$$x\Phi(x^2) = x \sum_{n=1}^{\infty} \exp\{-E_n x^2\} = G(x) \approx x^{-1} \sum_{j=0}^{\infty} K_j x^j \tag{13}$$

and differentiating m times. This eliminates the terms with coefficients $K_1, \ldots, K_m$, so that (denoting derivatives by superscripts in brackets)

$$[G(x)]^{(m)} \approx (-1)^m m! K_0 / x^{m+1} + m! K_{m+1} + \ldots . \tag{14}$$

Thus the limit

$$A = [4\pi(-1)^m / m!] \lim_{x\to 0} x^{m+1} \sum_{n=1}^{\infty} [x \exp\{-E_n x^2\}]^{(m)} \tag{15}$$

is approached with error of order $x^{m+1} = t^{(m+1)/2}$, and depends on the coefficient K_{m+1}.

This procedure is easily generalised to a means for systematically reconstructing all the coefficients K_j. From (13) we obtain

$$x^{-1}[xG(x)]^{(k)}/k! \approx x^{-1} \sum_{j=0}^{\infty} K_{k+j}[(k+j)!/j!\,k!]x^j. \tag{16}$$

This has the same form as (13) but with the leading coefficient K_k rather than K_0. Differentiating m times therefore gives the generalisation of (15) as

$$K_k = [(-1)^m / k!\,m!] \lim_{x\to 0} x^{m+1}[x^{-1}[xG(x)]^{(k)}]^{(m)} \tag{17}$$

where the limit is approached with error x^{m+1} and depends on the coefficient K_{k+m+1}.

For practical calculation, a convenient way to write these formulae is

$$K_k = \lim_{t\to 0} K_{k,m}(t) \tag{18}$$

where $K_{k,m}(t)$, *the mth approximant function for the kth coefficient*, is

$$K_{k,m}(t) = [(-1)^m/m!k!] \sum_{n=1}^{\infty} E_n^{(k/2-1)} \xi_n^{m+1} [\xi_n^{-1} [\xi_n^2 \exp\{-\xi_n^2\}]^{(k)}]^{(m)} \qquad \xi_n \equiv (tE_n)^{1/2}. \tag{19}$$

Equations (18) and (19) are the main results of this paper. Before discussing them, explicit formulae will be given for few $K_{k,m}(t)$.

For the area, (19) gives

$$A_m(t) \equiv 4\pi K_{0,m}(t) = (2\pi/m!)t \sum_{n=1}^{\infty} [\exp\{-\xi_n^2\} \xi_n^{m-1} H_{m+1}(\xi_n)] \qquad \xi_n \equiv (tE_n)^{1/2} \tag{20}$$

when H_{m+1} denotes the Hermite polynomials (Gradshteyn and Ryzhik 1965). The first few approximants are

$$A_0(t) = 4\pi t \sum_{n=1}^{\infty} \exp\{-E_n t\} \tag{21a}$$

$$A_1(t) = 4\pi t \sum_{n=1}^{\infty} \exp\{-E_n t\}(2E_n t - 1) \tag{21b}$$

$$A_2(t) = 4\pi t \sum_{n=1}^{\infty} \exp\{-E_n t\} E_n t(2E_n t - 3) \tag{21c}$$

$$A_3(t) = 4\pi t \sum_{n=1}^{\infty} \exp\{-E_n t\} E_n t(4E_n^2 t^2 - 12E_n t + 3)/3 \tag{21d}$$

For the length, (19) gives

$$L_m(t) \equiv -8\pi^{1/2} K_{1,m}(t)$$

$$= (8\pi^{1/2}/m!)t^{1/2} \sum_{n=1}^{\infty} [\exp\{-\xi_n^2\} \xi_n^m \{H_{m+1}(\xi_n) - (m+2)H_m(\xi_n)\}]$$

$$\xi_n \equiv (tE_n)^{1/2}. \tag{22}$$

The first few approximants are

$$L_0(t) = 16(\pi t)^{1/2} \sum_{n=1}^{\infty} \exp\{-E_n t\}(E_n t - 1) \tag{23a}$$

$$L_1(t) = 32(\pi t)^{1/2} \sum_{n=1}^{\infty} \exp\{-E_n t\} E_n t(E_n t - 2) \tag{23b}$$

$$L_2(t) = 16(\pi t)^{1/2} \sum_{n=1}^{\infty} \exp\{-E_n t\} E_n t(2E_n^2 t^2 - 7E_n t + 2). \tag{23c}$$

For the constant term, (18) gives (with $C_m(t) \equiv K_{2,m}(t)$)

$$C_0(t) = \sum_{n=1}^{\infty} \exp\{-E_n t\}(2E_n^2 t^2 - 5E_n t + 1) \tag{24a}$$

$$C_1(t) = \sum_{n=1}^{\infty} \exp\{-E_n t\}(4E_n^3 t^3 - 16E_n^2 t^2 + 7E_n t + 1) \tag{24b}$$

$$C_2(t) = \sum_{n=1}^{\infty} \exp\{-E_n t\}(4E_n^4 t^4 - 24E_n^3 t^3 + 23E_n t^2 + E_n t + 1). \tag{24c}$$

For the first post-constant term, (18) gives (with $D_m(t) \equiv 3K_{3,m}(t)/2$)

$$D_0(t) = -t^{-1/2} \sum_{n=1}^{\infty} \exp\{-E_n t\} E_n t (2E_n^2 t^2 - 9E_n t + 6) \tag{25a}$$

$$D_1(t) = -2t^{-1/2} \sum_{n=1}^{\infty} \exp\{-E_n t\} E_n^2 t^2 (2E_n^2 t^2 - 13E_n t + 15). \tag{25b}$$

Reconstructions of the coefficients K_k via (18) and (19) have errors of order $t^{(m+1)/2}$ and so are expected to be more accurate for larger m; if the coefficient K_{k+m+1} on which the error depends happens to vanish, the corresponding approximation can be expected to be especially accurate (we shall see several examples of this in the next sections).

Nevertheless, it is unrealistic to expect accuracy to continue to improve indefinitely with m. To understood why, it will be sufficient to consider the area approximants $A_m(t)$, which from (20) can be written as

$$A_m(t) = 4\pi t \sum_{n=1}^{\infty} g_m(E_n t) \tag{26}$$

where

$$g_m(\tau) = \tau^{(m+1)/2} \exp\{-\tau\} H_{m+1}(\tau^{1/2})/2m!. \tag{27}$$

Note first that the functions $g_m(\tau)$ all have area unity, i.e.

$$\int_0^{\infty} d\tau\, g_m(\tau) = 1. \tag{28}$$

However, as illustrated in figure 5, they oscillate with increasing amplitude as m increases: asymptotics of Hermite polynomials shows that $g_m(\tau)$ rises near $\tau = m$ to a maximum of order $\exp\{m^{1/2}\}/m^{1/2}$. Thus computation of a high-order approximant function $A_m(t)$ from the sum (26) requires the eigenvalues to be known with an error that decreases exponentially with m. In particular, such a computation would be ruined by including only a finite number N of eigenvalues in the term. To see this, note first

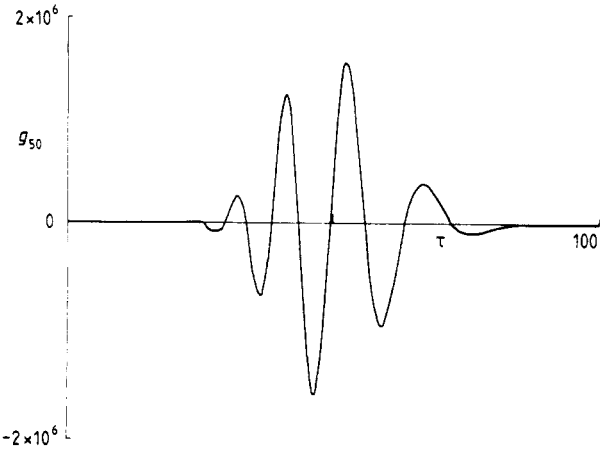

Figure 5. The function $g_{50}(\tau)$ (equation (27)) occurring in the 50th area approximant; note the large values near the maximum.

that reconstruction must employ eigenvalues $t \gg t_{N,m}$ where $t_{N,m} = \tau_m / E_N = m/E_N$ is the t for which the finiteness of N starts to seriously affect the value of $A_m(t)$. On the other hand, to reach the plateau for approximant error ε requires $t \ll t_{\varepsilon,m}$ where $t_{\varepsilon,m} = \varepsilon^{2/(m+1)}$ (because the error is of order $t^{(m+1)/2}$). Therefore the approximant technique works only whilst $t_{N,m} < t_{\varepsilon,m}$ and so must eventually fail because $t_{N,m}$ increases faster than $t_{\varepsilon,m}$.

3. Numerical illustrations

For each of the four billiards to be described below, approximant functions $K_{k,m}(t)$ were computed using the formulae (19)-(25) and their behaviour examined for small t. In almost all cases it was very easy to see how the smooth approach to the limit was frustrated by large and rapidly changing deviations caused by including only finitely many eigenvalues in the sums. The best approximation for K_k with a given approximant $K_{k,m}(t)$ was taken to be the extremum or inflection closest to the t value where the large deviations began. Table 1 summarises the results which will be discussed for the four billiards in turn.

Table 1. Accuracy of reconstructions using the approximant functions $K_{k,m}(t)$ of § 2 for the rectangular membrane (RM), Africa membrane (AM), Africa Aharonov-Bohm (AAB) and Africa neutrino (AN) billiards, computed using 125 eigenvalues for RM, AM and AAB and 181 eigenvalues for AN. All quantities except those marked * are given as percentage errors.

		Billiard			
Approximant		RM	AM	AAB	AN
Area	$A_0(t)$	22	17	17	0.6
	$A_1(t)$	2	1.4	0.5	0.8
	$A_2(t)$	$<10^{-9}$	0.1	0.07	0.08
	$A_3(t)$	$<10^{-9}$	0.01	0.02	0.01
Length	$L_0(t)$	14	10	4	0.5*
	$L_1(t)$	$<10^{-4}$	1	0.7	0.05*
	$L_2(t)$	$<10^{-4}$	0.03	0.2	0.02*
Constant	$C_0(t)$	$<10^{-7}$	12	38	−0.1*
	$C_1(t)$	$<10^{-7}$	1.2	3.5	−0.08*
	$C_2(t)$	—	—	—	−0.09*
Post-constant	$D_0(t)$	$<10^{-8}$ *	—	—	—

3.1. *Rectangle membrane billiard*

Let the sides of the rectangle have lengths $r^{1/2}$ and $r^{-1/2}$, so that the ratio of side lengths is r and

$$A = 1 \qquad L = 2(r^{1/2} + r^{-1/2}). \tag{29}$$

The first three coefficients K_j in the power series (8) for $\Phi(t)$ are given by (9) and (3). In particular, because all four angles β_i are $\pi/2$ and the curvature is zero the constant

term is

$$C = \tfrac{1}{4}. \tag{30}$$

It is a remarkable feature of the rectangular membrane that all the higher coefficients are zero. This follows from an exact expression for $\Phi(t)$ which will now be obtained.

The eigenvalues of $-\nabla^2$ for this membrane are

$$E_{mn} = \pi^2(m^2 r + n^2/r) \qquad 1 < m, n < \infty \tag{31}$$

so that

$$\Phi(t) = \sum_{m=1}^{\infty} \sum_{n=1}^{\infty} \exp[-\pi^2 t(m^2 r + n^2/r)]. \tag{32}$$

This is a product over Jacobi's θ_3 functions (Gradshteyn and Ryzhik 1965) and his identity (or Poisson's summation formula) gives

$$\Phi(t) = \tfrac{1}{4}\left(1 - (r/\pi t)^{1/2} - 2(r/\pi t)^{1/2} \sum_{m=1}^{\infty} \exp(-m^2 r/t)\right)$$
$$\times \left(1 - (1/\pi r t)^{1/2} - 2(1/\pi r t)^{1/2} \sum_{m=1}^{\infty} \exp(-m^2/rt)\right). \tag{33}$$

When multiplied out, this gives precisely the series (8) with $K_{j \geq 3} = 0$, plus corrections vanishing exponentially with t (the exponents have the form $l^2/4t$ where l is the length of the non-isolated geodesics that close after m bounces on each side of length $r^{1/2}$ and n bounces on each side of length $r^{-1/2}$).

In this billiard the geodesics are integrable: the rectangular membrane has no classical chaos.

The side ratio $r = 2^{1/4}$ was chosen (making r^2 irrational and the E_{mn} non-degenerate), and the approximant functions calculated using the lowest 125 eigenvalues (it would have been easy to compute more, but for the Africa billiards to be discussed in the next two subsections only 125 were available and it was thought sensible to keep the different cases as similar as possible).

Consider first the area approximants $A_m(t)$. As is clear from table 1 and figure 6, the lowest such function $A_0(t)$ gives a poor estimate of A. This is because its error is

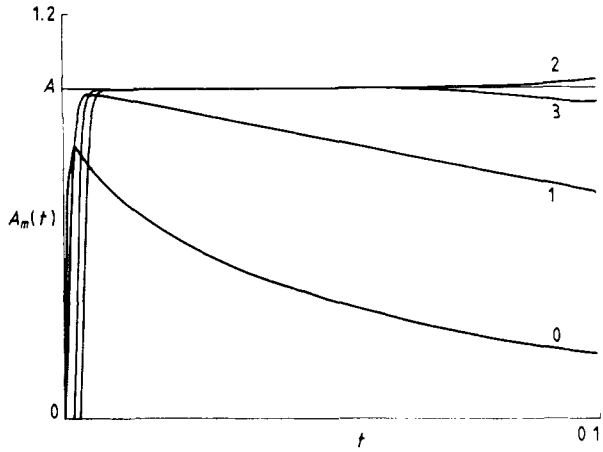

Figure 6. Area approximant functions $A_m(t)$ (equations (21)) for 125 eigenvalues of the rectangular membrane billiard with side ratio $2^{1/4}$, and unit area, for $m = 0, 1, 2, 3$.

dominated by the 'length' term and is of order $t^{1/2}$. A tenfold improvement is produced by $A_1(t)$; now the error is dominated by the 'constant' term and is of order t. With the next two approximants the improvement is dramatic, because these depend on the 'post-constant' coefficients K_3 and K_4 which are zero; the errors are therefore exponentially small in t rather than of order $t^{3/2}$ and t^2.

Table 1 and figure 7 show that the length approximants $L_m(t)$ behave similarly, except that now the dramatic improvement occurs with $L_1(t)$ because this depends on the first vanishing coefficient K_3.

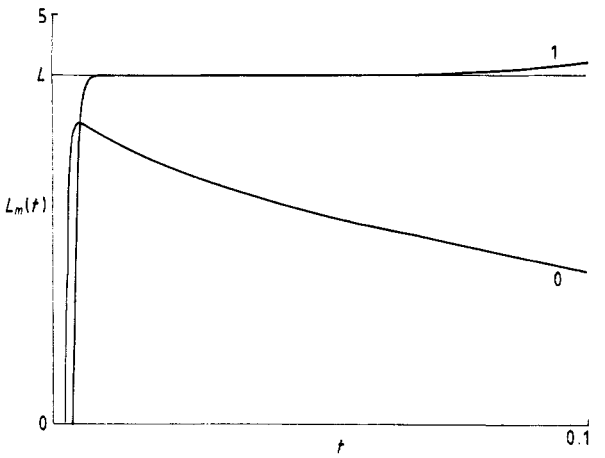

Figure 7. Length approximant functions $L_m(t)$ (equations (23)) for the billiard of figure 6 ($L = 4.0150$) for $m = 0, 1$.

For the constant term $C = \frac{1}{4}$, it is the lowest approximant $C_0(t)$ that gives exponential accuracy (nine digits in fact). This is far superior to the result obtained with the staircase fluctuations (6), for which the data (analogous to those in figure 2) give the average 0.233 (the fluctuations exceed this value by about five and their cumulative averages $\Sigma_{m=1}^{n} \Delta_m / n$ themselves fluctuate with an amplitude of about $C/5$).

Finally, table 1 confirms that $D_0(t)$, depending as it does on $K_4 = 0$, gives the expected exponential convergence onto the value (zero) of the first post-constant coefficient K_3.

3.2. Africa membrane billiard

To explore the 'curvature' contribution of the constant term in (3) without the complication of additional contributions from corners it is necessary to choose a billiard for which B is smooth. Such boundaries are easily generated by polynomial conformal maps of the unit circle (Robnik 1983, 1984). In addition, as explained by Berry and Robnik (1986) the simplest such map for which B has no symmetry is cubic; in the xy plane, with B parametrised by the angle ϕ round the unit circle,

$$x(\phi) + iy(\phi) = \exp\{i\phi\} + B_2 \exp\{2i\phi\} + B_3 \exp[i(\chi + 3\phi)] \qquad 0 \leq \phi \leq 2\pi \tag{34}$$

where B_2, B_3 and χ are all real and non-zero. From the various shapes thus generated we choose the 'Africa' shown in figure 8, for which $B_2 = B_3 = 0.2$, $\chi = \pi/3$. In this billiard, geodesics are not only non-integrable but probably completely chaotic (the

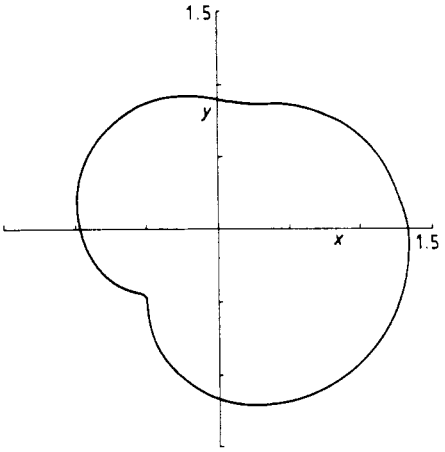

Figure 8. Africa billiard boundary, calculated from (34) with $B_2 = B_3 = 0.2$, $\chi = \pi/3$.

concave section of B is a powerful source of irregularity, and numerical evidence indicates ergodicity). From (34) and (3) it follows that

$$A = 3.769\,91 \qquad L = 7.101\,23 \qquad C = \tfrac{1}{6}. \tag{35}$$

The approximant functions $K_{k,m}(t)$ of equation (19) were computed using 125 membrane eigenvalues obtained by the conformal diagonalisation technique of Robnik (1984).

Results for the lowest four area approximants $A_m(t)$ are shown in table 1 and figure 9. None of the coefficients K_k vanish for this billiard, which therefore shows how the approximant technique works in a typical situation. Each successive approximant improves the estimate of A by about an order of magnitude. The 'length' and 'constant' approximants behave similarly, as figures 10 and 11 illustrate.

As already mentioned, these striking improvements cannot continue indefinitely because of the finite number of eigenvalues in the sums. Figure 9 shows what happens: as m increases, the plateau value occurs for larger t, and will eventually be reached

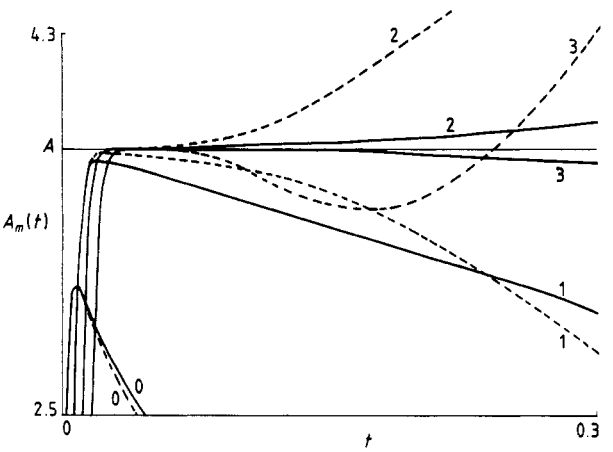

Figure 9. Area approximant functions $A_m(t)$ (equations (21)) for 125 eigenvalues of the Africa membrane billiard (full curves) and Africa Aharonov-Bohn billiard with golden flux ($\alpha = \frac{1}{2}(\sqrt{5}-1)$) (broken curves) for $m = 0, 1, 2, 3$.

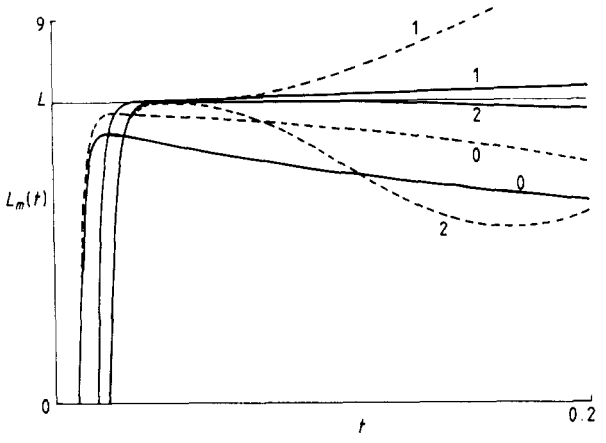

Figure 10. As figure 9 but for 'length' approximant functions $L_m(t)$ for $m = 0, 1, 2$.

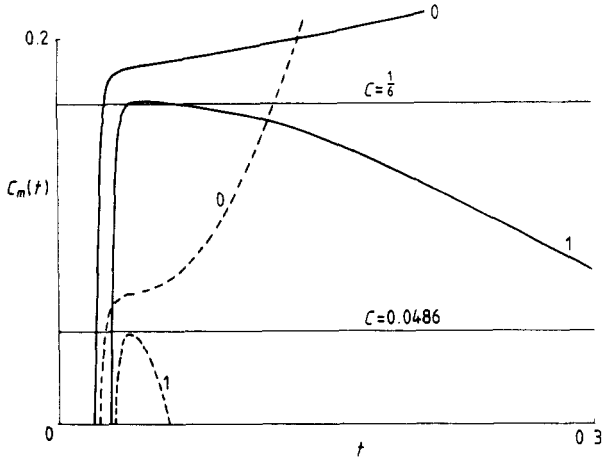

Figure 11. As figure 9 but for 'constant' approximant functions $C_m(t)$ for $m = 0, 1$.

before $K_{k,m}(t)$ begins to converge onto K_k. The number m of useful approximants decreases with k. For the constant, $C_2(t)$ (not shown) misses C by about 5%, and for the first post-constant coefficient K_3 even the lowest approximant $D_0(t)$ misses the target (equation (10)) by a factor of two.

3.3. Africa Aharonov-Bohm billiard

The boundary B is the same as in the previous subsection, but now a single line of magnetic flux threads the domain. We take this flux to be (in quantum units) the golden number $\alpha = (\sqrt{5}-1)/2 = 0.618\ldots$. For this billiard, 125 eigenvalues were computed by the method explained by Berry and Robnik (1986).

With flux, quantal time reversibility is broken. This has a profound effect on the statistics of the spectral fluctuations (Berry and Robnik 1986) but leaves the area and length asymptotics unaltered. However, the constant term is changed: from (4) we predict

$$C = 0.0486 \tag{36}$$

instead of $\frac{1}{6}$. As we shall demonstrate now, this change has a predictable effect on the behaviour of the approximant functions.

For the area approximants, figure 9 shows that the functions $A_0(t)$ are very similar for Africa with and without flux, but $A_1(t)$, $A_2(t)$ and $A_3(t)$ are different. The reason is that the convergence of $A_0(t)$ is determined by the length term, which is the same with and without flux, whereas the convergence of the higher approximants depends on higher coefficients, which are different with and without flux.

The same argument leads to the expectation that all the length approximants will differ considerably with and without flux, and figure 10 confirms that they do.

Of course, for the constant C it is not only the convergence but the values that differ, and figure 11 and table 1 show that the approximant technique succeeds in unambiguously distinguishing the two values.

Table 1 shows that the overall improvement of the estimates of K_k is roughly the same as for the Africa membrane, but the best estimates are less good (especially for L).

3.4. Africa neutrino billiard

For this relativistic billiard, 181 eigenvalues were computed by a boundary integral technique explained by Berry and Mondragon (1987). Although without flux, the billiard does not possess quantal time-reversal symmetry and the spectral fluctuations behave accordingly. The reason for including neutrino billiards in the present study is different: the factor γ in the length correction in (2) is zero (instead of unity as for all the other billiards) and this must affect the approximants.

It is clear from table 1 and figure 12 that the lowest approximant gives a much better estimate of A for neutrino billiards than for membrane or Aharonov-Bohm billiards. This is because the error in $A_0(t)$ depends on the 'length' term, which is zero in this case. For subsequent approximants this advantage disappears, and indeed their errors are comparable with those of the other Africa billiards.

Because $\gamma = 0$, the first few length approximants should converge on zero, and table 1 and figure 13 show that they do.

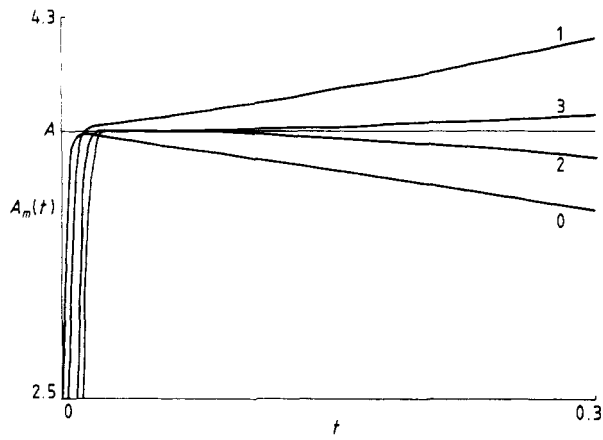

Figure 12. Area approximant functions $A_m(t)$ (equations (21)) for 181 eigenvalues of the Africa neutrino billiard for $m = 0, 1, 2, 3$.

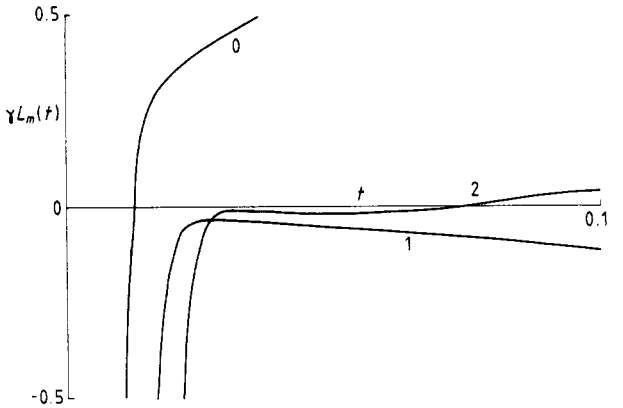

Figure 13. As figure 12 but for the 'length' approximant functions $L_m(t)$ for $m = 0, 1, 2$.

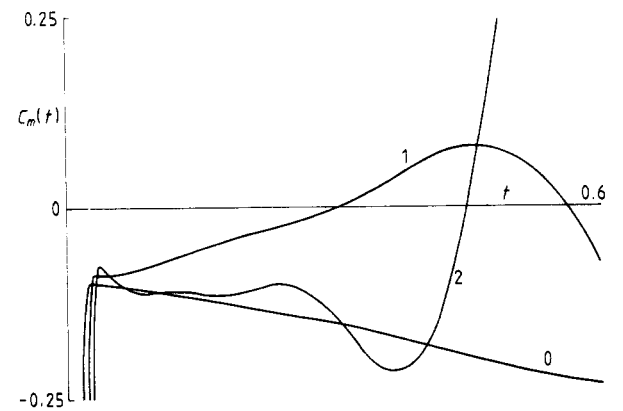

Figure 14. As figure 12 but for the 'constant' approximant functions $C_m(t)$ for $m = 0, 1$.

For the constant term there is as yet no theory; the first three approximants (table 1 and figure 14) suggest $C \approx -0.09$.

4. Discussion

This paper has been based on the simple trick, explained in § 2, of differentiating the partition function $\Phi(t)$ so as to knock out successive correction terms when approximating the coefficients K_k, thereby accelerating the approach to the limit as $t \to 0$. The same idea must surely have been employed by many people in many contexts, but I have been unable to find a reference in the literature. It certainly is effective: the billiard area can be approximated to one part in 10^4 from only 125 levels in a typical case (the Africa membrane). Such accuracy could not be obtained directly from the staircase $N(E)$—any attempt to employ for large E the same technique as was used here on $\Phi(t)$ for small t would founder because the steps would generate delta functions when differentiated. Of course this simply reflects the fact that in $N(E)$ the asymptotic fluctuations are large and oscillatory, whereas in $\Phi(t)$ they are exponentially small.

Classically integrable systems have larger spectral fluctuations than classically chaotic ones. This led Balazs and Voros (1987) to conjecture that reconstructions of the asymptotic coefficients in (2) or (8) (and more generally the spectral zeta functions $\Sigma_{n=1}^{\infty} E_n^{-s}$ continued to negative s) from a finite number of eigenvalues will be easier in the chaotic case. This is certainly true for reconstructions based on $N(E)$ but not for our much more accurate procedure based on $\Phi(t)$. Indeed in the particular integrable system studied here (rectangular membrane) the vanishing of all $K_{k\geq 3}$ enabled A to be reconstructed to one part in 10^{11} in spite of the large spectral fluctuations! In fact, what determined the accuracy of our reconstructions of a given coefficient K_k was not the classical chaology but the values of the next few coefficients. I do not know whether this remains true as the number of included eigenvalues and the order m of reconstruction both increase indefinitely.

Acknowledgments

I thank Mr R Mondragon for supplying the three sets of Africa eigenvalues. This work was not supported by any military agency.

References

Balazs N L and Voros A 1987 *Phys. Rep.* to be published
Balian R and Bloch C 1972 *Ann. Phys., NY* **69** 76-160
Baltes H P and Hilf E R 1976 *Spectra of Finite Systems* (Mannheim: B-I Wissenschaftsverlag)
Berry M V 1981 *Ann. Phys., NY* **131** 163-216
—— 1985 *Proc. R. Soc.* A **400** 229-51
—— 1986 *J. Phys. A: Math. Gen.* **19** 2281-96
Berry M V and Mondragon R 1987 *Proc. R. Soc.* to be published
Berry M V and Robnik M 1986 *J. Phys. A: Math. Gen.* **19** 649-68
Chazarain J 1974 *Invent. Math.* **24** 65-82
Gradshteyn I S and Ryzhik I M 1965 *Table of Integrals, Series and Products* (New York: Academic)
Kac M 1966 *Am. Math. Month.* **73**(4) Part 2 1-23
Robnik M 1983 *J. Phys. A: Math. Gen.* **16** 3971-86
—— 1984 *J. Phys. A: Math. Gen.* **17** 1049-74
Stewartson K and Waechter R T 1971 *Proc. Camb. Phil. Soc.* **69** 353-63